GEOPHYSICAL RESEARCH LETTERS, VOL. 28, NO. 23, PAGES 4449-4452, DECEMBER 1, 2001

PMCs and the water frost point in the Arctic summer mesosphere

Michael H. Stevens, Robert R. Conway, Christoph R. Englert

E.O. Hulburt Center for Space Research, Naval Research Laboratory, Washington, DC

Michael E. Summers

School of Computational Sciences, George Mason University, Fairfax, VA

Klaus U. Grossmann, Oleg A. Gusev

Department of Physics, University of Wuppertal, Wuppertal, Germany

Abstract. In August, 1997 the Middle Atmosphere High Resolution Spectrograph Investigation (MAHRSI) obtained vertical profiles of OH number density and polar mesospheric cloud (PMC) brightness by scanning the limb up to 71° N while the Cryogenic Infrared Spectrometers and Telescopes for the Atmosphere (CRISTA) obtained co-located vertical profiles of temperature. MAHRSI OH densities are converted to water vapor using a one-dimensional model that assumes photochemical equilibrium. By combining water vapor profiles with CRISTA temperatures we map the frost point both vertically and horizontally in the Arctic summer mesosphere. Our data show that supersaturation can exist between 80-87 km suggesting that growth of ice particles is limited to these altitudes. Additionally, we find that not only is supersaturation an insufficient condition for a PMC but also that PMCs can exist in apparently unsaturated air.

1. INTRODUCTION

PMCs are observed near 82 km around the summer pole and their composition was recently confirmed to be water ice *[Hervig et al., 2001]*. Although simple models of cloud condensation show that PMCs exist only where water vapor is supersaturated, this premise has never been tested with simultaneous observations of clouds, temperature and water vapor *[Thomas, 1991]*. In fact, cloud evolution models and certain observations suggest that supersaturation is not a good test for the presence of an ice cloud *[Jensen and Thomas, 1994; Lübken et al., 1996]*. Because optically active ice particles vary on time scales of hours *[Klostermeyer, 1998]*, near simultaneous observations of temperature, water vapor and PMCs are required.

Summers et al. [2001] recently discovered a narrow (<5 km) water vapor layer with peak concentrations of over 10 ppmv at PMC altitudes in the Arctic summer using OH results from MAHRSI and water vapor results from the Halogen Occultation Experiment on the Upper Atmospheric Research Satellite. They argued that this layer is due to the vertical redistribution of water vapor through growth and decay of PMCs.

Paper number 2001GL013598.
0094-8276/01/2001GL013598$05.00

Here we infer the distribution of water vapor around PMCs in the Arctic as well as the first co-located profiles of temperature, OH and PMCs. The co-located observations are a 17 minute snapshot of data with high vertical resolution from CRISTA-SPAS (Shuttle Pallet Satellite). We infer temperatures from CRISTA observations of CO_2 ν_2 band intensities near 15 μm and OH densities and PMC brightnesses from MAHRSI observations of the (0,0) band and backscattered sunlight near 309 nm. Using a one-dimensional photochemical model we then calculate water vapor profiles from OH densities, determine the regions of supersaturation and compare them to the PMC observations. We discuss the results in the context of ice particle growth and sedimentation.

2. EXPERIMENTAL APPROACH

From August 8-16 1997, CRISTA and MAHRSI flew for the second time on the CRISTA-SPAS, deployed and retrieved by the space shuttle (STS-85). Scanning the limb independently, the two instruments observed the summer mesosphere at latitudes up to 71° N. CRISTA measured the infrared emission of a variety of species between 4-71 μm *[Offermann et al., 1999]* including 15 μm CO_2 emission from which temperature profiles may be inferred. CRISTA used three telescopes and the center one was bore-sighted with MAHRSI. MAHRSI measured the solar resonance fluorescence of hydroxyl (OH) near 309 nm while simultaneously measuring the UV sunlight scattered by PMCs along the line of sight.

CRISTA-SPAS was deployed into a 300 km circular orbit with an inclination of 57° and the spacecraft maintained a fixed local vertical attitude relative to the Earth's limb. At the highest northern latitudes the lines of sight were pointed north which allowed for observations of PMCs by MAHRSI between 62-71° N and 8-15 local time (LT). MAHRSI limb scans were executed as a step-stare sequence with each 2 km step at the tangent point followed by 4.4 s of integration. These operations allowed for the retrieval of OH densities in the PMC region at a scan rate that resulted in OH density profiles every 800 km down track. CRISTA also vertically sampled every 2 km but the scan rate was about a factor of two higher.

MAHRSI observed OH by measuring the solar resonance fluorescence of the $A\ ^2\Sigma^+ - X\ ^2\Pi$ (0,0) band with a spectral resolution of ~0.02 nm between tangent altitudes 93-40 km. Retrieval of the OH rotational emission envelope requires subtraction of the bright and spectrally complex Rayleigh

background. This background shape is scaled to each limb spectrum and subtracted to retrieve the OH radiances, which are inverted to infer vertical profiles of OH densities *[Conway et al., 1999]*. Vertical structures in each MAHRSI OH (water vapor) profile can be resolved to 4.7 km at 82 km.

At the highest latitudes of observation near 82 km, MAHRSI occasionally measured additional background emission due to sunlight scattered by PMC particles along the line of sight. The "clear air" background brightness and its standard deviation are derived using a group of 26 scans between longitudes -80° E and -20° E where PMC scattering is not evident in the limb spectra. A PMC detection limit is herein defined as a background brightness that is in excess of 3σ above the clear air average, which is a scattering ratio (SR) of 1.2 at 82.0 km.

For the limb viewing geometry each measurement is an integral of all emission along the line of sight so lower tangent height observations can include PMC signals from higher altitudes. Because of this, we do not include every limb spectrum with excess scattering as a PMC detection. For scans with PMCs apparent at multiple tangent altitudes we only include as detections those measurements with excess scattering at and above altitudes of 80 km. A MAHRSI limb spectrum with a PMC is shown in the top panel of Figure 1 and the OH emission spectrum retrieved from the limb spectrum is shown in the bottom panel demonstrating that OH and PMCs can be measured simultaneously.

CRISTA temperatures are derived from CO_2 15 μm ν_2 band intensities using a Non-Local Thermodynamic Equilibrium (NLTE) model and radiative transfer code *[Kutepov et al., 1998]*. Besides the quantitative knowledge of the specific kinetic processes relevant to the excitation and quenching of the CO_2 molecules *[Shved et al., 1998; Ogibalov et al., 1998]*, several atmospheric parameters are required for the time and location of the sounding. Of major importance besides CO_2 itself are the concentrations of atomic oxygen because of its very high quenching cross-section for the ν_2 band levels of CO_2 *[Sharma and Wintersteiner, 1990]*. The atomic oxygen concentrations are determined indirectly from the NLTE retrieval of ozone assuming photochemical equilibrium between ozone and atomic oxygen *[Lary, 1991]*. CO_2 densities are derived from the measured 4.3 μm band intensities, as pumping by solar photons is the only excitation process of importance in the upper mesosphere during daytime. The background atmosphere is built up using the retrieved temperatures and assuming hydrostatic equilibrium.

A significant source of uncertainty in the temperatures is the rate constant for the collisional quenching of CO_2 by atomic oxygen. We use a rate constant of $k_0 = 3 \times 10^{-12}\ (300/T)^{½}$ [$cm^3 s^{-1}$] as recommended by *López-Puertas et al. [1998]* and assume an uncertainty of a factor of two. Other errors are due to the CO_2 mixing ratios, atomic oxygen densities, instrument calibration and noise.

The degree of saturation is given by $S=p_{H2O}/p_{sat}$, where p_{H2O} is the water vapor partial pressure and p_{sat} (in Pascals) is the saturation pressure of water vapor over ice, which may be written

$$p_{sat} = \exp[28.868 - 6132.935/T] \quad (1)$$

where T is in Kelvins *[Marti and Mauersberger, 1993]*. Equation (1) is derived from measurements of hexagonal crystalline ice down to 170 K and we assume here that it may be used for mesospheric ice down to 141 K *[Kouchi, 1987; Seele and Hartogh, 1999; Lübken, 1999]*.

3. RESULTS

Water vapor mixing ratio profiles are inferred from OH density profiles between 8.0 and 16.0 LT (>57° N) using the modeling technique described by *Summers et al. [2001]*. Figure 2 shows water vapor mixing ratios at 82.0 km inferred from 17 orbits of OH observations between August 13, 15 UT and August 14, 19 UT. Each square represents a different scan

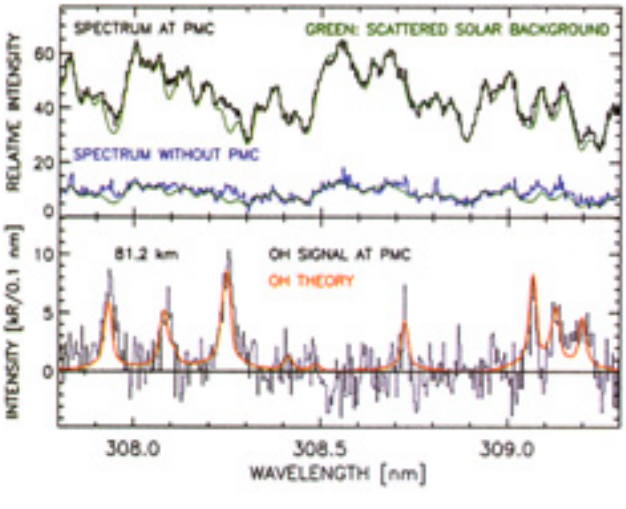

Figure 1. Top panel: A MAHRSI limb spectrum at 70.5° N and 11.8 LT taken on August 14 at 18.7 UT with PMCs along the line of sight (black histogram), and a spectrum at 68.1° N and 13.1 LT taken 127 s later without PMCs (blue histogram). Bottom panel: The OH spectrum inferred from the PMC limb spectrum by subtracting the background.

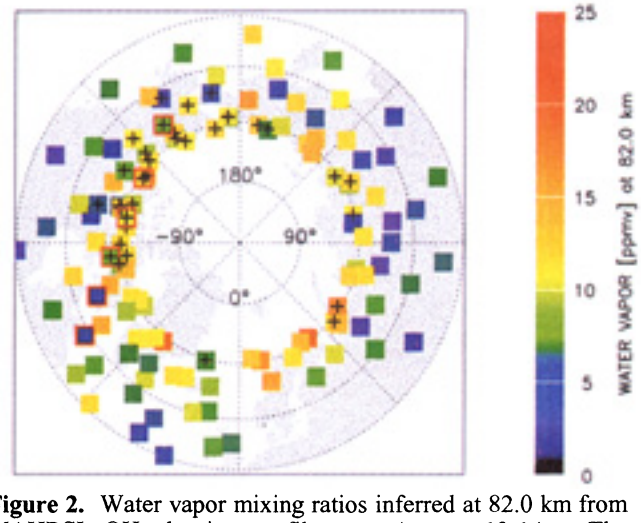

Figure 2. Water vapor mixing ratios inferred at 82.0 km from MAHRSI OH density profiles on August 13-14. The minimum latitude shown is 50° N, the latitude contour interval is 10° and no measurements were made poleward of 71° N. Squares with crosses indicate scans with PMCs and the squares outlined in red indicate sequential scans for which water vapor mixing ratios are combined with co-located CRISTA temperatures in Figures 3 and 4.

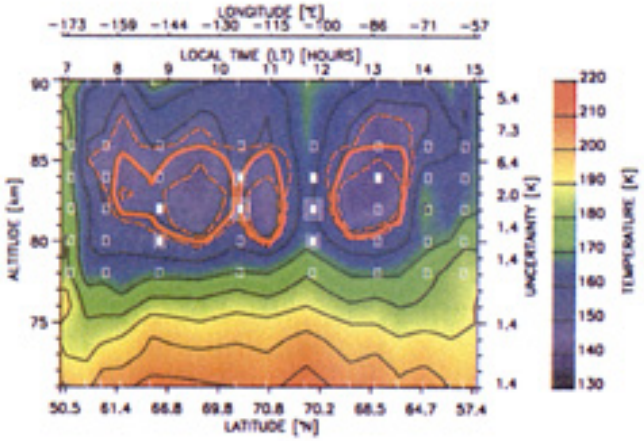

Figure 3. CRISTA temperatures measured on August 14 between 18.5 and 18.8 UT. The path described by latitude, longitude, and local time is the same as that by the outlined squares in Figure 2 and is referenced to an 82.0 km tangent altitude. The solid red contour is the frost point calculated using water vapor inferred from MAHRSI OH observations. Open symbols show a MAHRSI limb observation where the area subtended at the tangent altitude by the slit is approximately to scale. Solid symbols show a PMC detection with a background brightness of 1.2-2 times the clear air result, one box around the symbol is 2-4 times clear air conditions, and two boxes indicate the observation is 4-6 times clear air. CRISTA scan locations over which the image is interpolated are shown by tick marks on the inside border of the image and uncertainties are indicated on the right hand axis.

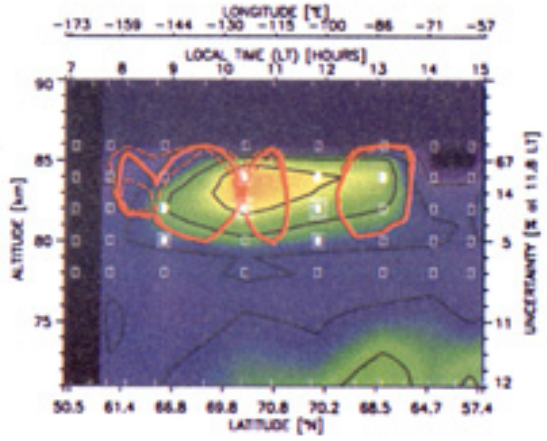

Figure 4. MAHRSI water vapor inferred from OH densities for the same time period and geographic region as the CRISTA data in Figure 3. The PMCs are observed between scattering angles 138-151°. Early in the orbital day the lighting conditions do not allow for reliable results for water vapor from OH so those results are not shown. Typical statistical uncertainties are indicated on the right hand axis.

and a cross within indicates that the scan includes unambiguous solar scattering along the line of sight by PMCs.

Figure 2 is distinguished by a region of enhanced water vapor poleward of 65° N where mixing ratios vary significantly between 3-23 ppmv with an average value of 12 ppmv. The variability is well beyond the propagated OH statistical uncertainty of 1 ppmv for any one of these points. There is no clear relationship evident between water vapor concentrations and PMC occurrence in the data shown. Although PMCs are apparently preferentially located between longitudes 170° E and -80° E in Figure 2, note that the map is a compilation of 27 hours of observations so that spatial and temporal variations are mixed. This is also important in the interpretation of the water vapor as the adjacent observations near 69° N and -40° E, for example, are 11 and 22 ppmv but inferred 24 hours apart.

Figure 3 shows retrieved CRISTA temperatures for the high latitude portion of one orbit displayed as a function of LT (top axis) and altitude. The salient feature of Figure 3 is the low mesopause between 82-85 km for the profiles from 7.5-14.0 LT *[von Zahn et al., 1996]*. S is calculated as a function of altitude by interpolating MAHRSI water vapor and CRISTA temperature profiles onto the same altitude and LT grid. The water frost point (S=1) contours are overplotted in red, encircling regions of S>1. Included in Figure 3 are dashed red contours, which show the frost point where the root sum square of systematic and statistical temperature uncertainties is propagated through the calculation. Also included in Figure 3 are midpoints of the MAHRSI tangent layers with PMC detections and relative brightnesses indicated.

Figure 4 shows the water vapor field used with the same solid frost point contour from Figure 3 included. The dashed contours indicate how statistical uncertainties in OH densities change the frost point through the inferred water vapor. An upper limit of 1 ppmv was used at 86 km where photochemical equilibrium between water vapor and OH begins to break down *[Summers et al., 2001]*. We assume the same upper limit between 86-90 km where we cannot detect OH emission to a 2σ limit for any of the profiles in Figure 4. Note that although statistical uncertainties in OH have a much smaller effect on the frost point than temperature, dehydration above 85 km limits the supersaturation there.

4. DISCUSSION

Figure 3 shows that for our data, supersaturation can exist between 80-87 km. Since the air between 87-90 km cannot sustain growth, the primary implication of this result is that sedimentation of ice particles from these altitudes is not important. Additional insight into PMC growth and decay may be gained by exploring the distribution of PMCs around the frost point contours in Figures 3 and 4.

The data show that not only can PMCs be absent where S>1 (13.1 LT, 82 km) but they may even exist where S<1 (11.8 LT, 80-84 km). Although it is possible that the PMC observed at 11.8 LT is from the near or far field, the 82.0 km SR is large at 4.3 (*cf.* Figure 1). If the near or far field path length were scaled to the tangent height path length, the cloud would be brighter than any included in Figure 2, strongly suggesting that the cloud exists in the tangent layer. However, the CRISTA profiles are limited to a vertical resolution of 2.2 km and a horizontal resolution of ~300 km so that if temperature structures were smaller than this and produced conditions locally cold enough for supersaturation, our only evidence might be scattering of sunlight by ice particles in path increments along the line of sight. Therefore although the temperature is an average for each tangent layer, it may be an upper limit when calculating S for a PMC parcel observed within the tangent layer.

Comparison of a 9 scan CRISTA average throughout the region of supersaturation in Figure 3 with a mid-August falling sphere (FS) temperature measurements in the Arctic summer

mesosphere *[Lübken, 1999]* shows that at 82 km the CRISTA average is 6.5 K lower whereas at 90 km CRISTA is 21 K higher. Using mid-August FS temperatures and model water vapor mixing ratios of 2.4-1.6 ppmv from 85-90 km *[Lübken, 1999]*, the water frost point is reached from 86-88 km ($1<S<2$). However, the dehydration inferred between 86-90 km unsaturates this region even without the higher CRISTA temperatures. Regardless of how much water vapor is between 86-90 km, the variability at 82 km of a factor of six (Figure 2) directly affects supersaturation and provides new constraints on models that describe the condensation and sublimation of PMCs.

5. SUMMARY

Using satellite-borne co-located observations of PMC brightness, temperature and OH on August 14, 1997 we find that water vapor supersaturation can exist between 80-87 km suggesting that growth of ice particles is limited to these altitudes. We also find that the observed PMC distribution is not exclusively determined by the measured saturation conditions of the tangent layers in which they reside. By combining vertical profiles of temperature, water vapor mixing ratio and PMC brightness, we find that PMCs do not necessarily exist in supersaturated air and conversely we find evidence that they can exist in unsaturated air. These results are consistent with those from a two-dimensional particle evolution model describing the microphysical effects of temperature perturbations in the upper mesosphere *[Jensen and Thomas, 1994]*.

Our data reveal an Arctic summer mesopause between 82-85 km and a layer of water vapor in the same region where concentrations vary substantially between 3-23 ppmv at 82 km. To constrain microphysical models, we find that the detailed vertical structure of both temperature and water vapor as shown by our data are required to reliably describe supersaturation in the Arctic summer mesosphere.

Acknowledgements. We thank J.G. Cardon for his assistance in analyzing the MAHRSI data and M. Rapp for many productive discussions on ice particle growth. Helpful comments on the manuscript by D.E. Siskind and S.D. Eckermann are also appreciated. The Office of Naval Research and the NASA Office of Space Science supported this research. This work was performed while C.R. Englert held a National Research Council - NRL Research Associateship.

REFERENCES

Conway, R.R., et al., Middle Atmosphere High Resolution Spectrograph Investigation, *J. Geophys. Res.*, *104*, 16,327-16,348, 1999.

Hervig, M., et al., First confirmation that water ice is the primary component of polar mesospheric clouds, *Geophys. Res. Lett.*, *28*, 971-974, 2001.

Jensen, E.J. and G.E. Thomas, Numerical simulations of the effects of gravity waves on noctilucent clouds, *J. Geophys. Res.*, *99*, 3421-3430, 1994.

Klostermeyer, J., A simple model of the ice particle size distribution in noctilucent clouds, *J. Geophys. Res.*, *103*, 28743-28752, 1998.

Kouchi, A., Vapour pressure of amorphous H_2O ice and its astrophysical implications, *Nature*, *330*, 550-552, 1987.

Kutepov A.A., O.A. Gusev, V.P. Ogibalov, Solution of the non-LTE problem for molecular gas in planetary atmospheres: Superiority of accelerated lambda iteration, *J. Quant. Spect. Rad. Trans.*, *60*, 199-220,1998.

Lary, D.J., Photochemical Studies With a 3D Model of the Atmosphere, Ph. D. Thesis, Cambridge University, 1991.

López-Puertas, M., G. Zaragoza, and M.Á. López-Valverde, Non local themodynamic (LTE) atmospheric limb emission at 4.6 μm 1. An update of the CO_2 non-LTE radiative transfer model, *J. Geophys. Res.*, *103*, 8499-8513, 1998.

Lübken, F.-J., Thermal structure of the Arctic summer mesosphere, *J. Geophys. Res.*, *104*, 9135-9149, 1999.

Lübken, F.-J., K.-H. Fricke, and M. Langer, Noctilucent clouds and the thermal structure near the Arctic mesopause in the summer, *J. Geophys. Res.*, *101*, 9489-9508, 1996.

Marti, J. and K. Mauersperger, A survey and new measurements of ice vapor pressure at temperatures between 170 and 250 K, *Geophys. Res. Lett.*, *20*, 363-366, 1993.

Ogibalov V.P., A.A. Kutepov, G.M. Shved, Non-local thermodynamic equilibrium in CO_2 in the middle atmosphere II. Populations in the $\nu_1\nu_2$ manifold states, *J. Atmos. Sol.-Terr. Phys.*, *60*, 315-329,1998.

Offermann, D. et al., Cryogenic Infrared Spectrometers and Telescopes for the Atmosphere (CRISTA) experiment and middle atmosphere variability, *J. Geophys. Res.*, *104*, 16311-16325, 1999.

Seele, C. and P. Hartogh, Water vapor of the polar middle atmosphere: Annual variation and summer mesosphere conditions as observed by ground-based microwave spectroscopy, *Geophys. Res. Lett.*, *26*, 1517-1520, 1999.

Sharma, R.D., and P.P. Wintersteiner, Role of carbon dioxide in cooling planetary thermospheres, *Geophys. Res. Lett.*, *17*, 2201-2204, 1990.

Shved G.M., A.A. Kutepov and V.P. Ogibalov, Non-local thermodynamic equilibrium in CO_2 in the middle atmosphere. I. Input data and populations of the ν(3) mode manifold states, *J. Atmos. Sol.-Terr. Phys.*, *60*, 289-314,1998.

Summers, M.E. et al., Discovery of a layer of enhanced water vapor in the Arctic summer mesosphere: Implications for polar mesospheric clouds, *Geophys. Res. Lett.*, *28*, 3601-3604, 2001.

Thomas, G.E., Mesospheric clouds and the physics of the mesopause region, *Rev. Geophys.*, *29*, 553-575, 1991.

von Zahn, U. *et al.*, The mesopause altitude: Only two distinctive levels worldwide?, *Geophys. Res. Lett.*, *23*, 3231-3234, 1996.

M. H. Stevens, R. R. Conway, and C. R. Englert, Code 7641, Naval Research Laboratory, 4555 Overlook Ave., Washington, DC 20375 (e-mail: stevens@uap2.nrl.navy.mil)

M. E. Summers, School of Computational Sciences, Department of Physics and Astronomy, and Center for Earth Observing and Space Research, George Mason University, MSN-5C3, Fairfax, VA 22030

K. U. Grossmann, O. A. Gusev, Department of Physics, University of Wuppertal, 42097 Wuppertal, Germany.

(Received June 8, 2001; revised August 27, 2001; accepted September 14, 2001.)

Correction to "PMCs and the water frost point in the Arctic summer mesosphere" by M. H. Stevens et al.

Received 8 February 2002; published XX Month 2002.

INDEX TERMS: 0305 Atmospheric Composition and Structure: Aerosols and particles (0345, 4801); 0340 Atmospheric Composition and Structure: Middle atmosphere—composition and chemistry; 0360 Atmospheric Composition and Structure: Transmission and scattering of radiation; 9315 Information Related to Geographic Region: Arctic region

[1] In the paper "PMCs and the water frost point in the Arctic summer mesosphere" by M.H. Stevens et al. [*Geophys. Res. Lett.*, 28, 4449–4452, 2001], Figure 4 was inadvertently printed without the accompanying color bar. The figure and its color bar appear below.

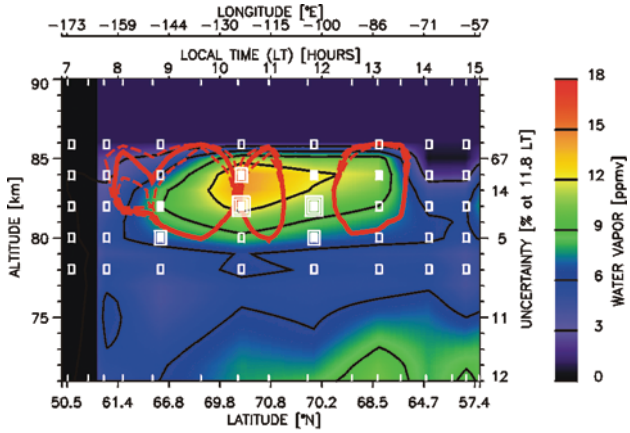

Figure 4. MAHRSI water vapor inferred from OH densities for the same time period and geographic region as the CRISTA data in Figure 3. The PMCs are observed between scattering angles 138–151°. Early in the orbital day the lighting conditions do not allow for reliable results for water vapor from OH so those results are not shown. Typical statistical uncertainties are indicated on the right hand axis.

0094-8276/02/2002GL014885$05.00